Cellulose (2023) 30:9349–9364
https://doi.org/10.1007/s10570-023-05443-x

ORIGINAL RESEARCH

Mechanistic analysis of nanocellulose formation tuned by deep eutectic solvents

Xuerong Bi · Jiansheng Guo · Jin Wen · Chongwen Yu

Received: 27 September 2022 / Accepted: 7 August 2023 / Published online: 24 August 2023

Abstract Clean energy and green solvents have attracted wide attention due to their non-toxic, biodegradable, and recyclable properties. Deep eutectic solvent (DES), as a green solvent, has advantages in the formation of nanocellulose. To reveal the formation mechanism during cellulose nanocrystal (CNC) preparation, different carboxylic acid DESs are compared in the optimal experimental conditions. Experimental observations show that oxalic acid (OA) DESs can fabricate CNCs with higher yield, higher crystalline index than that of citric acid series. Moreover, crystal water molecules in DESs promote the reaction activity of DESs in the CNC formation. To understand the interaction among the DES/cellulose complex, molecular dynamics simulations and quantum chemical calculations were applied to investigate the arrangement of CNCs in the atomic scale. The radial distribution function and intermolecular interactions indicate that the non-covalent intermolecular interactions between DESs and cellulose are strong, which could be further enhanced by the crystal waters in DESs. Reaction pathways during the formation of CNCs were revealed by computational simulations, which show that OA is more prone to react with cellulose in esterification and acidolysis reactions. Both computational and experimental results demonstrate that the OA DESs are more beneficial in the production of CNCs. The synergistic effects of chemical reactions and non-covalent interactions favor the formation of CNCs by DESs.

Keywords Cellulose nanocrystal (CNC) · Deep eutectic solvent (DES) · Molecular dynamics (MD) simulations · Quantum chemical calculation · Non-covalent interaction

Supplementary Information The online version contains supplementary material available at https://doi.org/10.1007/s10570-023-05443-x.

X. Bi · J. Guo · C. Yu (✉)
College of Textiles, Donghua University, Shanghai 201620, China
e-mail: yucw@dhu.edu.cn

J. Guo · C. Yu
Key Laboratory of Textile Science & Technology, Ministry of Education, Donghua University, Shanghai 201620, China

J. Wen (✉)
State Key Laboratory for Modification of Chemical Fibers and Polymer Materials, College of Materials Science and Engineering, Donghua University, Shanghai 201620, China
e-mail: jinwen@dhu.edu.cn

Introduction

Over the past decades, nanocellulose has attracted rapidly growing interest due to its excellent performance, such as high tensile strength, high elastic modulus, large specific surface area, and low density combined with biodegradability and renewability

(Moon et al. 2011; Rajinipriya et al. 2018). According to the morphology and formation techniques, cellulose nanomaterials mainly include cellulose nanocrystals (CNCs), cellulose nanofibrils (CNFs), and bacterial nanocellulose (BNC) (Du et al. 2019). Among all the formation methods of CNCs, strong acid hydrolysis is indeed a simple, common, and time-saving method (Cheng et al. 2017). However, problems such as harsh corrosion of equipment, severe environmental pollution, large water consumption, and relatively low production yield need to be well addressed (Xie et al. 2018). Some sustainable and environmentally friendly methods based on the replacement of the recyclable chemicals have been put forward recently to address the above drawbacks, such as solid acid hydrolysis (Liu et al. 2014; Torlopov et al. 2017), organic acid hydrolysis (Chen et al. 2016; Du et al. 2016; Xu et al. 2017), ionic liquid (Miao et al. 2016), or deep eutectic solvent (DES) treatment (Lim et al. 2021; Liu et al. 2017a, b; Selkälä et al. 2016; Sirviö et al. 2016).

Deep eutectic solvent has shown quite excellent performance in the nanocellulose formation. DES is composed of hydrogen bond donor (HBD) and hydrogen bond acceptor (HBA). Due to the strong hydrogen bond interaction between HBD and HBA, DES can easily form a uniform liquid at a relatively low temperature (Abbott et al. 2004). Among all kinds of DESs, acidic DESs possess the most advantage in preparing CNCs. Many researchers chose choline chloride as HBA, while oxalic acid, lactic acid, toluenesulfonic acid, and levulinic acid as HBD to prepare varieties of acidic DESs (Liu et al. 2017a, b; Sirviö et al. 2016). These DESs can effectively produce cellulose nanocrystals with diameters range from several to tens of nanometers. Previous works reported that the DES composed of oxalic acid/choline chloride could destroy the hydrogen bond network of cellulose by forming competing hydrogens bonding between DESs and cellulose (Liu et al. 2021; Liu et al. 2017a, b). However, this inference is a qualitative description based on experiment, the mechanism of the CNC formation by DESs has not been studied thoroughly yet. During the preparation of nanocellulose by DESs, two main reactions occurred. The one is esterification between carboxylic acid and hydroxyl group at the C6 position on cellulose, which makes cellulose fibers split into finer fibril. The other is acidolysis reaction under acidic conditions as β-1,4 glycosidic bond breakage, which makes cellulose fibers break along the longitudinal direction. Recently, fundamental research analyzed the interaction between DESs and cellulose molecules at the molecular level by quantum chemistry (Fu et al. 2020) and molecular simulations (Smirnov et al. 2020). Results demonstrated that the hydrogen bond interactions of the cellulose hydroxyl groups with the chloride ions were the key factors of the destruction of cellulose in the process of solvation. In addition, it has been shown that the interactions within the studied DESs are strengthened when low amounts of water existing (Kalhor et al. 2020). Moreover, Ahmadi et al. (Ahmadi et al. 2018) found that the hydrous DESs systems favored the formation of more hydrogen bonds by molecular dynamics simulations.

The properties of DESs would be changed by a few crystal water molecules in HBD so that the ability of CNC formation will also be affected. However, the effect of water molecules existing in DESs on CNC formation has not been studied in depth. It is necessary to investigate the differences between hydrous DESs and anhydrous DESs in the nanocellulose formation and the effect of water molecules during the formation process. In this work, two kinds of organic acid (with and without crystal water) were chosen to mix with choline chloride. The DESs were applied to the jute noil pretreatment and CNC formation. The non-covalent interaction and chemical reaction between DESs and cellulose was investigated by experiment and molecular simulations to reveal the effect of different DESs and water molecules on CNC formation.

Materials and methods

Experimental methods

Materials and chemicals

Jute noil fibers (the fibers wasted during the spinning process) were obtained from Xiangnan Jute Co.Ltd., Chenzhou, Hunan Province, China. All the chemicals including benzene, ethanol, sodium hydroxide (NaOH), sodium chlorite ($NaClO_2$), acetic acid (HAc), choline chloride (ChCl), oxalic acid (OA), oxalic acid dihydrate ($OA{\cdot}2H_2O$), citric acid (CA), and citric acid monohydrate ($CA{\cdot}H_2O$) were

purchased from Sinopharm Group and RON reagent, which were of analytical grade.

Pretreatment of jute noil fibers

Jute noil fibers were firstly treated by benzene/ethanol extraction to remove oil and wax. Then, further treated with 17.5 w/v% NaOH solution to remove hemicellulose and pectin. Subsequently, the treated samples were bleached with 0.7 w/v%. sodium chlorite ($NaClO_2$) to remove lignin, and treated at pH = 4 (HAc buffer solution) boiling for 2 h under a fiber to liquor ratio of 1:50 and then treated with 5 w/v% sodium hydrogen sulfite solution. Filtering, washing with distilled water, and drying at 60 ℃ in a vacuum oven until constant weight. The bleached jute fibers were preserved as raw materials for producing CNCs.

Formation of DES

The hydrogen bond donor (organic acid) and hydrogen bond acceptor (ChCl) were weighed at a molar ratio of 1:1. The DESs were prepared by mixing the HBA and HBD and heated over the eutectic point with a 500 rpm magnetic stirring until a transparent liquid formation. The molecular structures of HBA and HBD are shown in Fig. 1.

Formation of cellulose nanocrystals (CNCs)

The 1 wt% raw material (bleached jute fibers) were added to each DES and react at 90 °C for 5 h. After the DES treatment, the mixture of raw cellulose and DESs was dialyzed (dialysis tube with 8000 D cut-off) to neutral in deionized water. Then, the mixture was treated in an ultrasonic cell crushing apparatus (JY92-IIDN) for 30 min under the power of 600 W. After that, the mixture was centrifuged at 5000 rpm for 10 min and the supernatant contained CNCs was taken out. Finally, CNC suspensions were obtained, as shown in Fig. S1.

Characterizations

Yield rate of CNCs

The prepared CNC suspensions were dried and the weight of solid CNCs was measured. The yield rate was obtained as the average value of the sample measured three times.

Degree of polymerization

The average degree of polymerization (DP) of raw materials and CNCs was evaluated from the limiting viscosity, measured in copper ethylenediamine (CED)

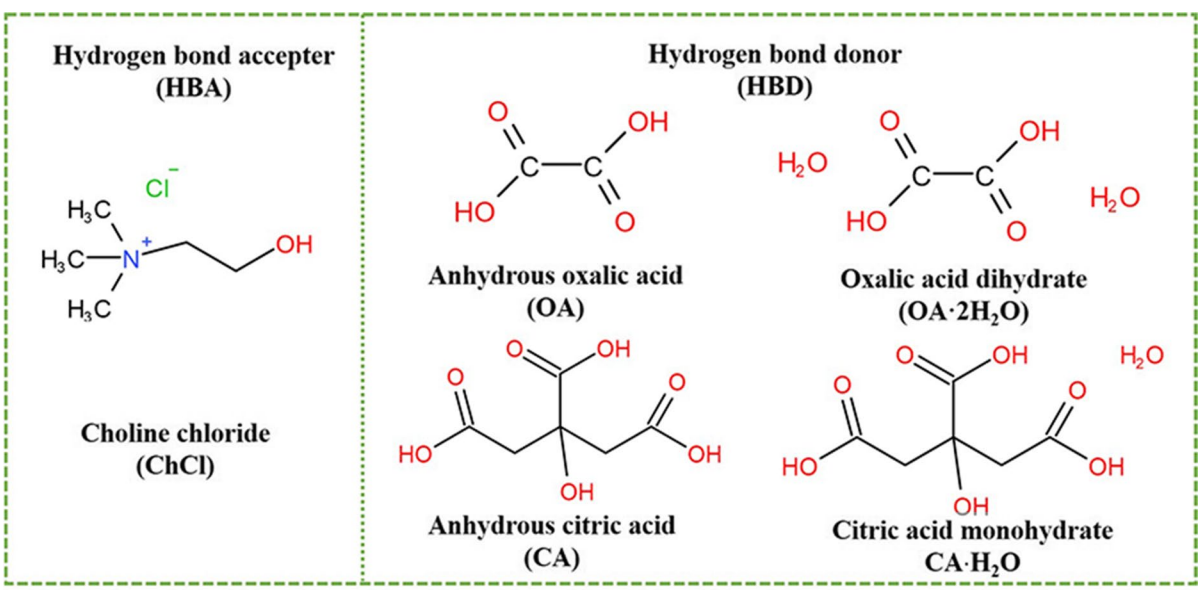

Fig. 1 The molecular structures of HBA and HBD

solution according to ISO 5351 standard. The DP was calculated by Eq. (1),

$$DP = \left(\frac{1.65[\eta] - 116H}{C}\right)^{1.111} \quad (1)$$

where $[\eta]$ was the limiting viscosity, C was the mass fraction of the sample, and H was the mass fraction of hemicellulose. For CNCs, H was assigned as 0.

Transmission electron microscopy (TEM)

TEM was used to observe the resulting nanocelluloses under a Transmission Electron Microscopy (JEM-2100, Japan) at 200 kV. A 5 μL aliquot of the diluted slurry was dropped on a carbon-coated electron microscopy grid (400 mesh). The sizes of the nanocelluloses were measured from the TEM images using the imageJ analysis system.

X-ray diffraction (XRD)

X-ray diffraction (XRD) analysis was used to test the crystallinity of the raw materials and CNCs. The samples were analyzed using a Bruker D8 Advance. XRD patterns were recorded from $2\theta = 5 \sim 60°$ with a D/max-RB diffractometer equipped with a graphite monochromator and Cu Kα radiation at $\lambda = 0.154$ nm (40 kV, 40 mA). Reflection mode and fixed slits were adopted in the test. The relative crystalline index (CrI) was estimated using peak fitting method by MDI Jade 6. Linear fit was used for background processing, while the threshold $\sigma = 4.0$ and K-α1/α2 ratio = 2.0. The peak deconvolution was adopted to calculate the CrI with pseudo-Voigt function (1.5 Exponent and 0.5 Lorentzian). The fitting peaks of $2\theta \approx 18°$ and 38° were defined as the amorphous region of cellulose.

Fourier transform infrared spectroscopy (FTIR)

FTIR spectra were recorded using a Nicolet 6700 spectrometer (Thermo Fisher, America) with a diamond attenuated total reflectance (ATR) attachment. The data were recorded over the range $400 \sim 4000$ cm^{-1} in absorbance mode with 32 scans per spectrum and with a resolution of 4 cm^{-1}.

^{13}C CP/MAS Nuclear Magnetic Resonance Spectrum (CP/MAS ^{13}C-NMR).

^{13}C CP/MAS NMR analysis on the raw materials and CNCs have carried out at room temperature with the AVANCE400 (Switzerland) spectrometer. Spectra were acquired with a 4 mm MAS probe using a combination of CP, MAS, and high-power proton decoupling methods. A total of 800 scans were accumulated for each sample.

Computational simulations

Details in molecular dynamics simulations

Models of cellulose in four DESs were constructed by Packmol package (Martínez et al. 2009), containing 400 DES molecules and 2 cellulose chains with the consistent-valence forcefield (CVFF) (Dauber-Osguthorpe et al. 1988). The system was obtained by geometry optimization, followed by an equilibrium process in an NPT ensemble in 5 ns with the time step of 1 fs when the temperature was set as 333 K by Materials Studio 6.0. The productions were carried out in the NPT ensemble, when the pressure was 0.0001 GPa during a total simulation of 5 ns. The radial distribution function (RDF) between different particles was analyzed according to the trajectories, which were collected every 1 fs.

Computational details in non-covalent interaction

Kohn–Sham DFT has become one of the most popular tools in electronic-structure theory due to its excellent cost-performance ratio (Kohn et al. 1996). DFT was employed to further investigate the interactions between cellulose and DESs in this work. Since cellobiose was the element of the polysaccharide cellulose, it was chosen to estimate the non-covalent interactions among the cellulose and its interaction with solvents in a simplified model. B3LYP functional (Becke 1988; Lee et al. 1988) with 6-311G(d,p) (Hariharan et al. 1973; Hehre et al. 1972) basis set was used to fully optimize the structures of DESs and cellobiose with the dispersion correction (Grimme et al. 2010). By comparing electronic energies of several initial structures, the most stable geometry was obtained, confirmed by the following frequency calculations. To investigate the polarizability of the DES/cellobiose complexes, electrostatic potential (ESP) was further plotted onto the isosurface with the electron density of 0.001 a.u. (Cao et al. 2016), shown

in Fig. S7. M062X functional (Zhao et al. 2008) with 6–311 + G(2d,p) (Frisch et al. 1984) basis set was used to calculate the electronic energy of DES/cellobiose complexes, which have correctly described non-covalent interactions, especially hydrogen bond interactions (Fu et al. 2020). Based on the optimized structures, reduced density gradient (RDG) and atoms in molecules (AIM) analyses were applied to demonstrate the non-covalent interactions of the DES/cellobiose complex (Tognetti et al. 2008). All DFT calculations were performed using the Gaussian 09W Revision D.01 software package (Frisch et al. 2016).

Binding energy analysis

The initial configuration of the complex was constructed according to the equilibrium state obtained from MD simulations. The calculation was accomplished at the level of M062X/6–311 + G(2d, p)//B3LYP/6-311G(d,p) with the dispersion correction(GD3).

The binding energy between DESs and cellobiose, ΔE can be defined as the following equation,

$$\Delta E = E_{\mathrm{C-DES}} - E_{\mathrm{C}} - E_{\mathrm{DES}} \quad (2)$$

where $E_{\mathrm{C\text{-}DES}}$ is the electronic energy of the DES/cellobiose complex, E_{C} and E_{DES} are electronic energies of cellobiose and DESs, respectively.

Atoms in molecules (AIM) analysis

AIM theory elucidates that the electron density (ρ), and laplacian density ($\nabla^2\rho$) can describe the properties of the hydrogen bond. Molecule plots are depicted by Multiwfn (Lu and Chen 2012) and VMD program (Lu and Chen 2021). According to the Espinosa-Molins-Lecomte equation (Espinosa et al. 1998), the relationship between V_{CP} and E_{HB} is $E_{\mathrm{HB}} = V_{\mathrm{CP}}/2$, where V_{CP} is potential density.

Reduced density gradient (RDG) analysis

In the aspect of the intermolecular interactions, the RDG method is a powerful tool to investigate the intermolecular interactions in DES/cellobiose complexes, including hydrogen bond, halogen bond, and π-π stacking, even the steric hindrance (Johnson et al. 2010). To present the intensity of these interactions, a scatter diagram of RDG with sign(λ_2)ρ projected onto the RDG isosurfaces was applied to illustrate the non-covalent interactions using Multiwfn and VMD programs (Lu and Chen 2021).

Reaction mechanism of cellulose in DESs

The Nudged Elastic Band (NEB) method (Mills and Jónsson 1994) is an algorithm to search the minimum energy path (MEP) in potential energy surface (PES) based on the interpolation between two energy minima. To identify reaction paths along esterification and acidolysis reactions, NEB method with semiempirical implementation GEN2-xTB(Bannwarth et al. 2019) was employed, which was carried out by ORCA 5.0 program(Neese 2012, 2022). The corresponding reactant, product, and transition state geometries were further optimized to obtain the reaction barrier at the B3LYP-D3BJ/cc-pVDZ level.

Results and discussion

Characterization of CNCs

The yield rate of CNCs is the main index to evaluate the performance of DESs in CNC formation, as presented in Table 1. It is obviously shown that the yield rate of CNC1 and CNC2 (producing by OA DESs) are ten times higher than that of CNC3 and CNC4 (producing by CA DESs). This result shows that OA DESs is more efficient in CNC formation. In addition,

Table 1 Composition of DESs and yield rate of prepared CNCs

Serial of DESs	HBA/HBD	Eutectic point (℃)	Pka of HBD	Serial of CNCs	Yield rate of CNCs (%)
DES1	ChCl/OA	28	1.23	CNC1	71.25
DES2	ChCl/OA·2H_2O	− 42		CNC2	76.3
DES3	ChCl/CA	69	3.13	CNC3	5.35
DES4	ChCl/CA·H_2O	54		CNC4	8.35

hydrous DESs can obtain a little more CNCs than that of anhydrous DESs. This result indicates that the type of HBD and the crystal water of HBD have an impact on the preparation of CNCs. The key of the preparation of CNCs using acidic DESs lies in two aspects: the disruption of cellulose hydrogen bonds by DESs leading to fibrillation, and the chemical reaction between the acid in DESs and cellulose (Liu et al. 2021). OA has a lower pka than CA so that the H^+ of OA can release easily. Therefore, cellulose hydrolyzed by OA is more vigorously. This may be one of the reasons for the high yield of CNCs produced by OA series DESs. And the presence of water molecules promotes the release of H^+ from HBD, which catalyzes acidolysis and esterification reactions to get higher yield rate.

TEM images and diameter distribution of cellulose nanocrystals produced with different DESs are shown in Fig. 2. The diameters of the CNCs are mostly ranged from 10 to 35 nm as well as the CV value is all around 30%. It is shown that the CNCs made by anhydrous DESs (DES1, DES3) get a finer diameter (19.5 nm) than that of hydrous DESs (DES2, DES4). The results show that although hydrous DESs are beneficial to increasing the yield rate of CNCs, it might be not profitable to get CNC diameter refinement. As to anhydrous DESs, the hydrogen bond dissociation effect is stronger, so the cellulose fiber is more significantly defibrillated to get finer diameter. The H^+ on the organic acid in the hydrous DESs is more easily released due to the exiting of water, so the catalytic hydrolysis reaction of cellulose is more significant. Under this effect, the diameter of the CNCs made by the anhydrous DESs is smaller.

The WAXD diffractograms presented in Fig. 3a indicate that the cellulose I and II crystalline structure all exist in the raw materials and CNCs. The main 2θ diffraction angles close to 14.9°, 22.6° and 34.8° are associated with cellulose I, while 12°, 20° and 22.1° are associated with cellulose II (French 2014). The fitting peaks of $2\theta \approx 18°$ and 38° were defined as the amorphous region of cellulose (French 2020). Peak deconvolution is used to calculate crystallinity with pseudo-Voigt function. Detailed peak fitting process were shown in Fig. S2–Fig. S6. Besides, the crystallinity index (CrI) of raw materials and CNCs as well as the DP of CNCs are shown in Fig. 3b.

According to Fig. 3b, the CrI of four kinds of CNCs all increase compared to the raw materials due to the amorphous region removal. Among them, CNC1 and CNC2, which are prepared by DES1 and DES2, obtained higher CrI than that of CNC3 and CNC4. This may be caused by the fact that OA is more inclined to acidolysis reaction with cellulose, resulting in a less amorphous region and higher crystallinity. This deduction is verified by the results of the DP value. When the crystallinity was higher, the DP of CNCs was lower, indicating that the amorphous region of cellulose was more fractured. The crystallinity of CNCs produced by hydrous DESs is slightly higher than that of anhydrous DESs. This indicates that the presence of crystal water molecules might promote organic acids release of more H^+ to a certain extent, and the proton can effectively catalyze the hydrolysis reaction of cellulose.

FTIR spectroscopy results in Fig. 4a show that cellulose characteristic peaks, including -OH stretching adsorption around 3420 cm^{-1}, $–CH_2$ symmetric bending around 1320 cm^{-1} to 1420 cm^{-1} and C–O–C stretching around 1064 cm^{-1}, existed in all CNCs and raw materials. This suggests that the major structures of cellulose are still retained after the treatment with different DESs. The esterification of cellulose can take place with the presence of carboxylic acids on the surface of CNCs. Compared with the spectrum of the raw materials, all the CNCs prepared by carboxylic acid DESs exhibited a new band around 1730 cm^{-1}, which is a peak of the carbonyl vibrations. In addition to carbonyl and hydroxyl stretching frequencies, methylene stretching frequencies centered at 2900 cm^{-1} are increased of DES modified CNCs (Spinella et al. 2016).

The structure elucidation of prepared CNCs was performed using ^{13}C CP/MAS NMR spectroscopy, as shown in Fig. 4b. The representative signals between 60 and 120 ppm were assigned to cellulose, in which 105 ppm corresponds to C1 of cellulose, 89 ppm corresponds to the crystal region of C4, 84 ppm corresponds to the amorphous region of C4, 72 ppm, 75 ppm corresponds to C2, C3 and C5 of cellulose, 65 ppm corresponds to crystal region of C6 and 62 ppm corresponds to the amorphous region of C6. The typical cellulose carbon peaks position remained unchanged after the DES pretreatment and the ultrasonication process. However, the CNC peaks of crystal regions of C4, C6, and peaks of C2, C3, C5 become more distinct. This result is consistent with Fig. 3. The crystal region of raw materials was

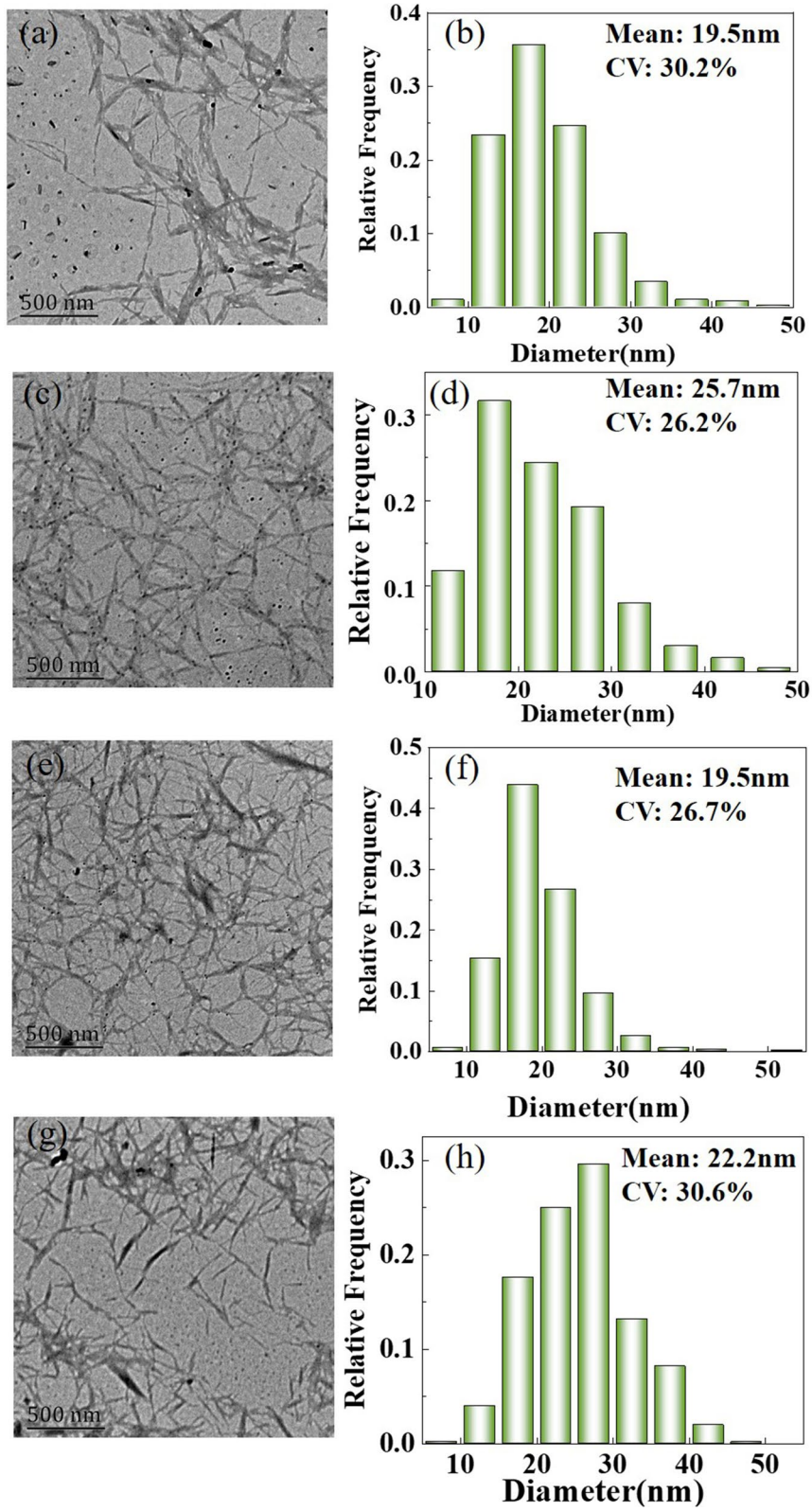

Fig. 2 TEM images and diameter distribution of CNCs produced with different DESs (**a**)–(**b**) CNC1; (**c**)–(**d**) CNC2; (**e**)–(**f**) CNC3; (**g**)–(**h**) CNC4

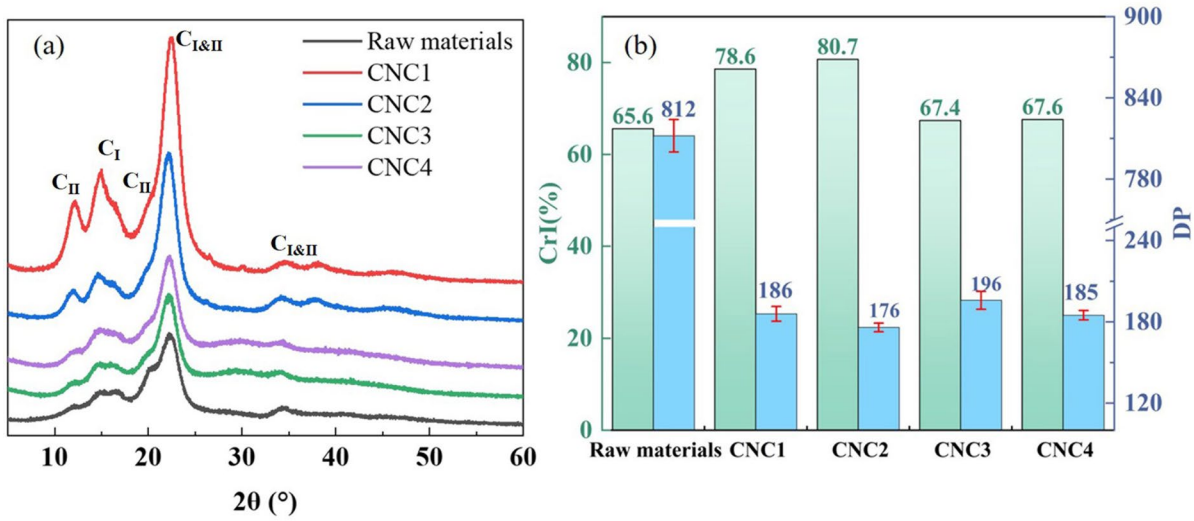

Fig. 3 XRD Diffractograms (**a**), CrI and DP (**b**) of CNCs

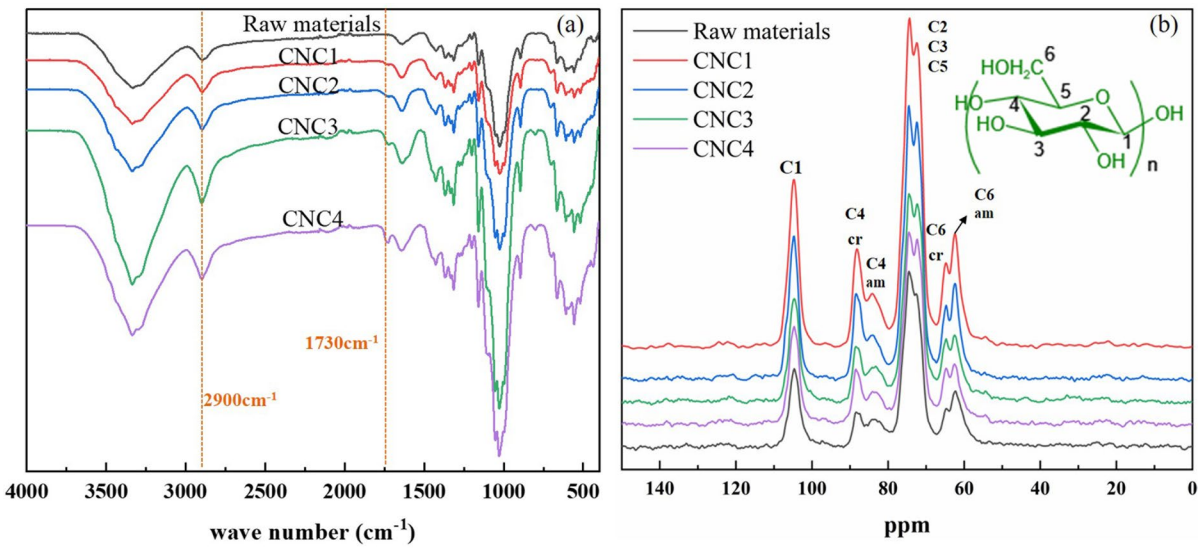

Fig. 4 The FTIR (**a**), and ^{13}C-NMR (**b**) of CNCs

exposed after DES treatment while the amorphous region was removed.

Solvation Effect on Packing Conformations of CNCs.

In order to understand the microscopic structure of the cellulose and DESs mixtures as well as the effect of composition and water content on the hydrogen bonding network, we simulated the packing structures of four DESs by molecular dynamics simulations. The radial distribution function (RDF) is an important function to characterize the microstructure, which can observe the distribution of atoms of DESs around the cellulose. Illustrative snapshots of the mixtures, as well as plots of RDFs, are shown in Fig. 5 and Fig. S8.

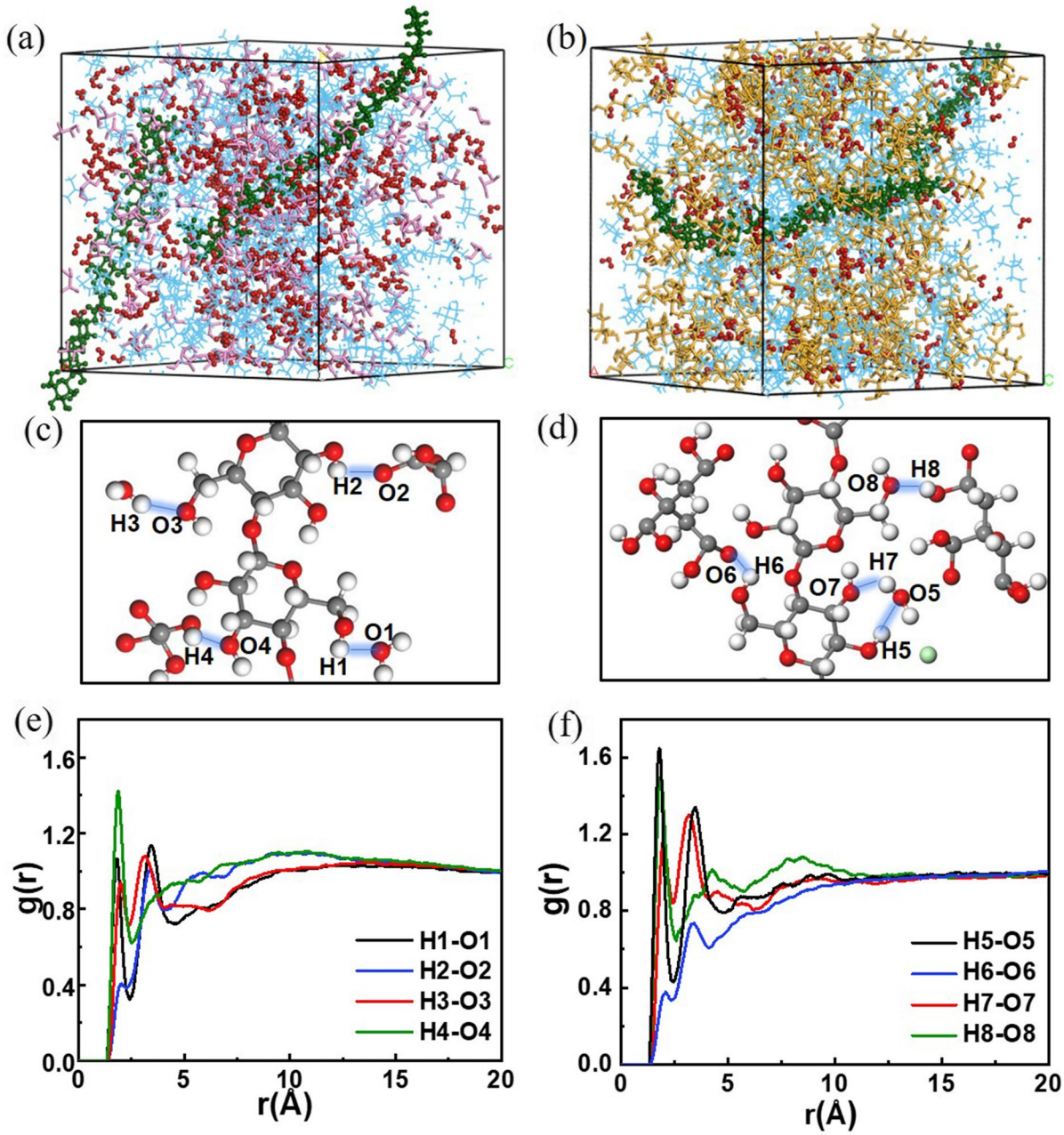

Fig. 5 Snapshots (**a**–**d**) and RDFs (**e**–**f**) of different DES/cellulose systems. Analysis in DES2/cellulose chains are presented in left column (**a**), (**c**), and (**e**); DES4/cellulose chains are presented in the right column (**b**), (**d**), and (**f**). (ChCl, blue; OA, pink; CA, yellow; water, red; cellulose, green)

The yield rate in Table 1 demonstrates that DES1 and DES2 are more beneficial in the formation process of CNCs. The comparison in the yield rate between DESs including crystal water and DESs without crystal water reveals that the crystal water contributes to the HBD, which makes CNC production more favorable. For hydrous DESs systems (Fig. 5), H_2O molecules in the systems have an obvious effect on hydrogen bond interaction. For DES2/cellulose systems in Fig. 5e, the first peak in the

hydrogen interaction of H4-O4 is at 1.89 Å, similar to the distributions of cellulose-water hydrogen bonds H1-O1 and H2-O2 at 1.85 Å and 2.07 Å, respectively. The hydrogen bond between cellulose and water molecules is the key factor, since the first peak of H5-O5 at 1.81 Å is the closest, followed by the first peaks of H8-O8 and H6-O6 at 1.91 Å and 1.99 Å respectively in the DES4 as shown in Fig. 5f. For the hydrogen distributions in H5-O5 and H6-O6, it is found that two significant peaks in RDF, indicating that the addition of water molecules increases the hydrogen bond interaction for CNC formation, agree with the trend of yield rate in Table 1. On the other hand, the strongest interaction is O_c-H_{OA} with the first peak at 1.81 Å in RDF as shown in Fig. S8 for anhydrous DESs.

In order to quantitatively analyze the strength of interaction between different DESs and cellulose, the binding energies between DESs and cellulose were studied. Although, cellulose is a polymer with cellobiose as a repeating unit, two representative models, $(C_6H_{10}O_5)_2$ and $(C_6H_{10}O_5)_{10}$ with different DP were proposed for calculating the binding energy, as shown in Fig. 6 and Fig. S9, respectively. The intermolecular interactions of the two models were calculated based on the CVFF force field, shown in Table S1. By comparing the binding energies between DESs and cellulose models with different chain lengths, it can be seen that there is a similar trend between short and long-chain models. In all, the intermolecular interactions between cellulose and DESs increase with the increase of DP.

To get more accurate results in the binding energies, DFT was applied. The binding energies (ΔE) of the DES/cellobiose and cellobiose dimers are shown in Fig. 6. The optimized coordinates of complex were shown in Table S3. Considering the intermolecular interactions in the crystal structures of cellobiose, two configurations of cellobiose dimer are depicted in Fig. S10 (c) and (f), respectively. First, four DESs interact with cellulose stronger than that in the cellobioses dimers, as the binding energies of DES/cellobiose are all more negative than − 33.4 kcal/mol and − 24.4 kcal/mol for (010) and (100) configurations in cellobiose dimers. The stronger intermolecular interaction leads the binding energy more negative. These results indicate that the interactions between cellobiose dimer can be destroyed by all DESs effectively, which could fibrillate the cellulose in the process of obtaining cellulose nanocrystals. Additionally, hydrous DESs interact with cellulose stronger than do anhydrous ones. This result reveals that the existing bound water of HBD is beneficial for promoting the interactions of whole systems. The hydrous DESs can form more hydrogen bonds than anhydrous DESs because the water molecule displays both HBD and HBA in the complex system.

Atoms in molecules (AIM) is another useful method to investigate non-covalent interactions, which is based on the electron density distribution between two atoms to define the chemical structure of the system (Bader 1992; Zheng et al. 2016). Table S2 depicts the topological parameters at the bonding

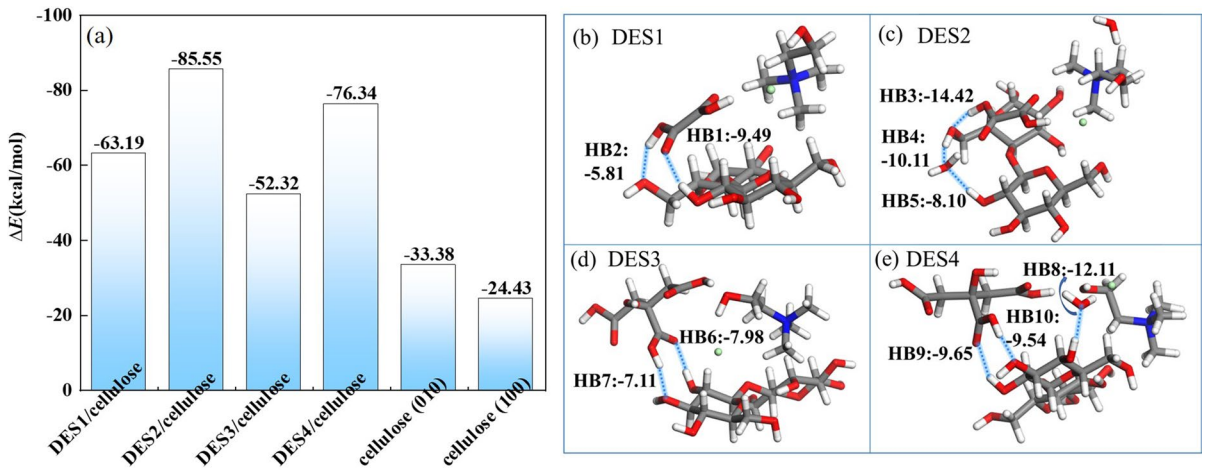

Fig. 6 The binding energies of DESs and cellobiose (**a**) and the major HBs interactions in different DES/cellobiose systems (**b**–**e**)

critical point (BCP) of interaction between various of DESs and cellobiose including electron density (ρ), the laplacian density ($\nabla^2\rho$), potential density (V_{CP}), and the energy of hydrogen bond (E_{HB}). The topological structures of different DES/cellobiose and cellobiose dimers are shown in Fig. S11. The positive $\nabla^2\rho$ value represents the presence of hydrogen bond interaction. According to Fig. 6, the E_{HB} of DES1 and DES2 is stronger than that of cellobiose dimer. Besides, the E_{HB} of DES3/cellobiose is slightly lower than the cellobiose dimer of (010) crystal face, which portends that the anhydrous DES3 shows the weaker ability for cellulose fibrillation. Moreover, a small amount of water molecules not only increase the hydrogen bond numbers, but also make the E_{HB} of the system increase significantly. This result also indicates the positive effect of the crystal water molecules in the hydrogen bond donor on the formation of CNCs.

Subsequently, RDG scatter diagrams and isosurfaces of different DES/cellobiose, as well as cellobiose dimer, were calculated and plotted in Fig. 7 and Fig. S10. The product of sign(λ_2)ρ is projected onto RDG isosurfaces with different colors to reveal the type and intensity of non-covalent interactions as well as to visualize non-covalent interactions by the VMD program. Here, the blue region indicates a strong interaction force (hydrogen bond), the green region shows weak interactions such as van der Waals forces, and the steric effect is distinguished by red. It can be clearly observed that there are prominent non-covalent interactions including hydrogen bond and van der Waals between DESs and cellobiose. Especially, existing crystal water molecules play an important role in HBA as well as HBD because the hydrogen can accept electrons while the oxygen can offer electrons, which were shown in Fig. 7d and h.

Reaction mechanism of DESs and cellulose

In anhydrous DESs, water molecules play the role as the products in the esterification. On the other hand, they are used as reactants in the acidolysis reaction, in which water molecules are consumed by the breakage of glycosidic bonds. Therefore, the esterification reaction can be promoted by the synergistic effect of acidolysis reaction. However, the esterification reaction is inhibited since water molecules act as the products when their concentration was increased in the case of hydrous DESs, as shown in Fig. 8a. Taking account of the overall interactions between DESs and cellulose, esterification and hydrolysis reactions have a synergistic effect during the formation of nanocellulose. The transition states of these two reactions were found through the NEB method, through which the structures of reactant, TS, and product are shown in Fig. S12. And the optimized coordinates of reactants, TS and products were shown in Table S4. The lower reaction barrier for the esterification reaction between OA and cellulose than that between CA and cellulose indicates that the esterification reaction is more likely to occur between OA and cellulose under the same reaction conditions, as shown in Fig. 8b. For the acid hydrolysis reaction, the reaction barrier of uncatalyzed was about 28 kcal/mol higher than the catalyzed ones, indicating that H^+ catalysis is critical in the acid hydrolysis reaction. For two organic acids, oxalic acid and citric acid, pKa are 1.23 and 3.13 for OA and CA respectively, which represents that the more acidic OA can released more H^+ in the solvent, so the acid hydrolysis reaction is more likely to occur in the DESs with OA. Considering these two factors, the acid hydrolysis and esterification reactions of DESs with OA and cellulose are dominant rather than the DESs with CA, which could explain the higher yield of CNCs prepared in the OA DESs.

Considering the results obtained from both experimental and computational observations, we propose the mechanism of the CNC formation in Fig. 9. The swelling of cellulose fibers is caused by the treatment of DESs, in which the hydrogen bonds of cellulose fibers dissociate, resulting in loose-packed cellulose fibers in the amorphous region. Subsequently, the organic acid in DESs breaks the amorphous region of cellulose fibers, leading to the formation of the cellulose nanocrystals. When a few water molecules existing in DESs, more competing hydrogen bond will form between cellulose and DESs. In summary, we deduce the cellulose fibers are fibrillated to form nanocellulose by the synergistic action of hydrogen-bonding dissociation and acid hydrolysis.

Conclusion

In this work, four DESs were applied to treat the wasted jute fibers in producing CNCs with the same experimental conditions. The prepared CNCs were

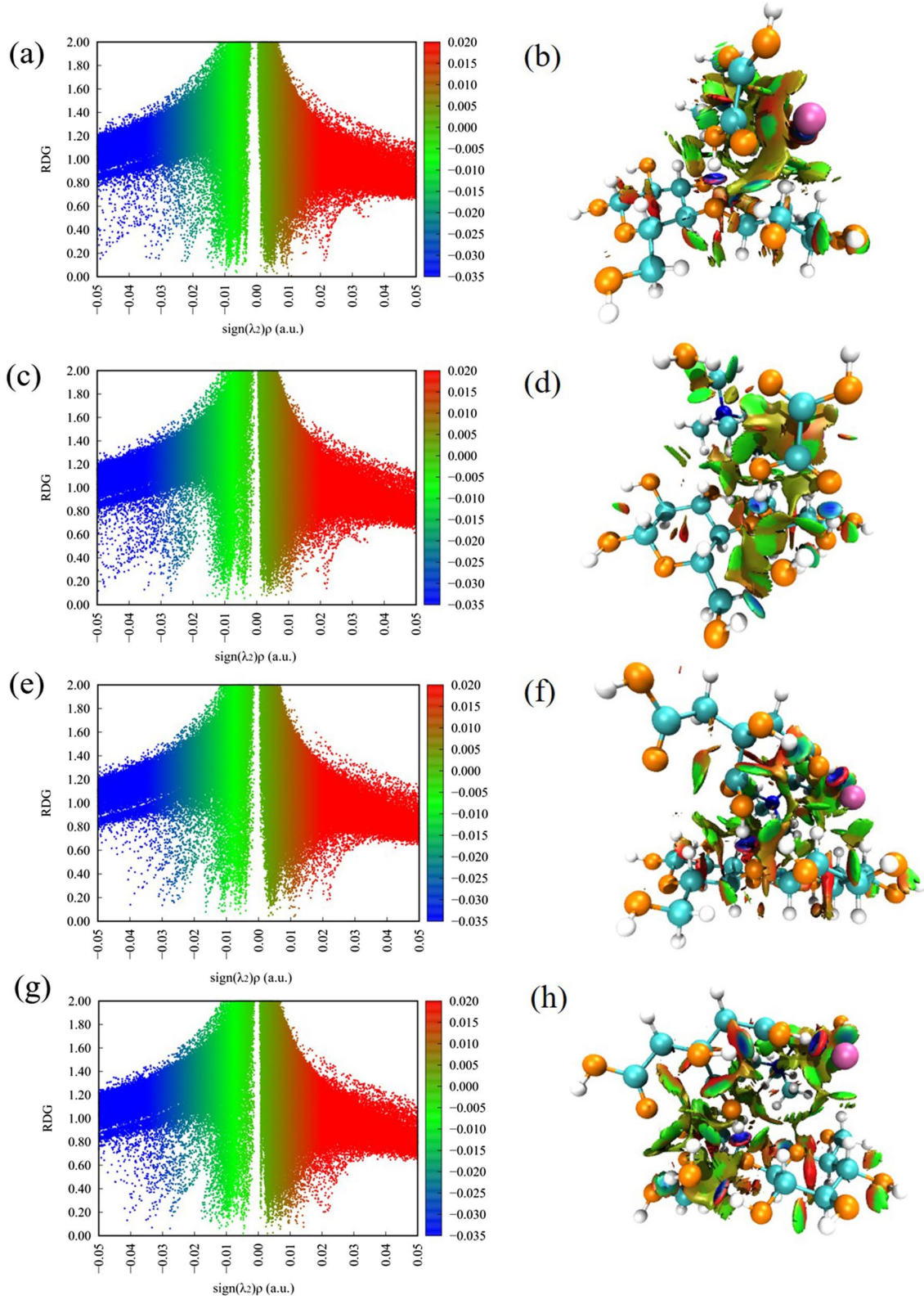
(a)
(b)
(c)
(d)
(e)
(f)
(g)
(h)
RDG
sign(λ2)ρ (a.u.)

◂**Fig. 7** RDG analysis of different DES/cellobiose. Isosurfaces are colored over the range from -0.035 a.u. to 0.02 a.u. **a–b** DES1/cellobiose, **c–d** DES2/cellobiose, **e–f** DES3/cellobiose, and **g–h** DES4/cellobiose

investigated by the XRD, TEM, FTIR, and ^{13}C-CP/MAS NMR. Among these DESs, OA series show a visible superiority in producing CNCs over CA series. Based on the analysis of the yield rate and CrI of the production, it can be found that the organic acid which contains crystal water molecules can promote the performance of DESs in producing CNCs. Molecular dynamics simulations were applied to perceive the intermolecular interactions on the microscopic scale. RDF, which was analyzed based on the dynamic trajectories, demonstrates the non-covalent interaction between DESs and cellulose is strong. RDG and AIM analyses reveal that the hydrogen-bonding and van der Waals interactions between DESs and cellulose are the key factors in the fibrillation of cellulose. Furthermore, a small amount of water molecules in the DESs enhance the intermolecular interaction due to the

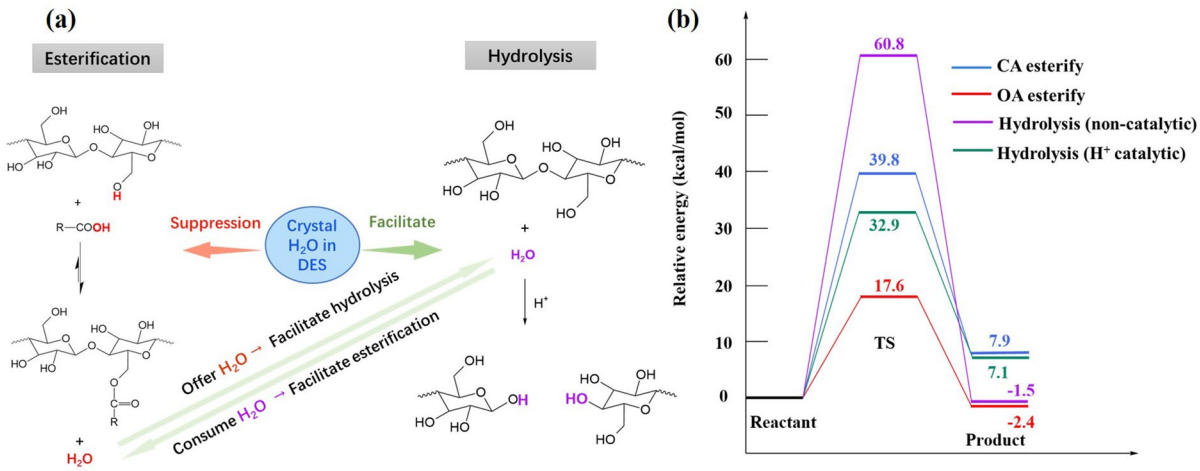

Fig. 8 **a** Chemical reactions between cellulose and DESs, and **b** relative energies (in kcal/mol) along the reaction path

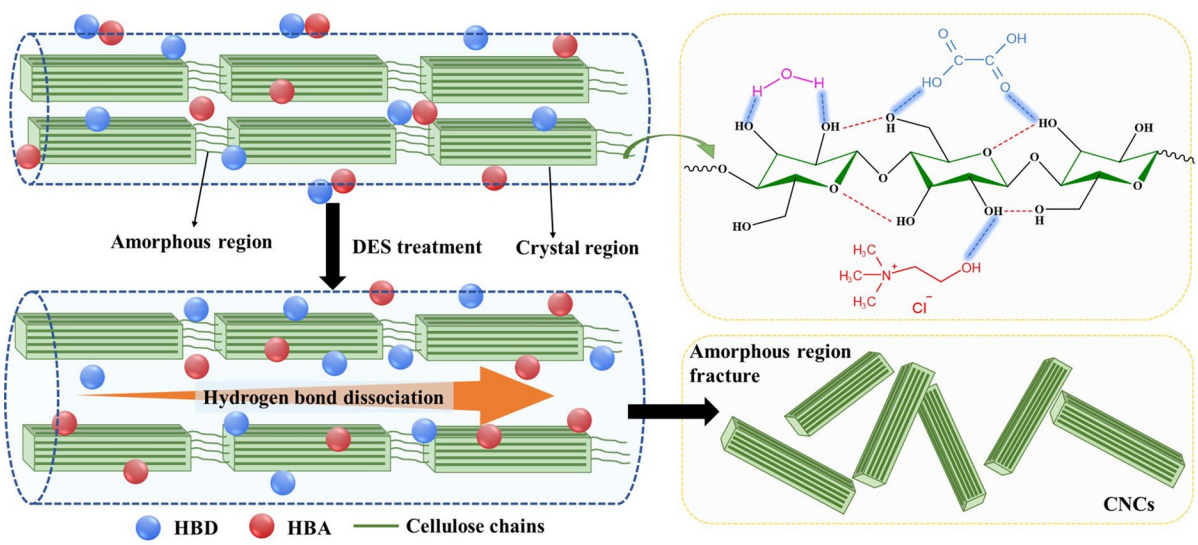

Fig. 9 Predicted mechanism of CNCs prepared by DESs

additional formation of hydrogen bonds within the complex. The computational simulations in the involved reactions showed that the esterification and acidolysis reactions between OA DESs and cellulose were more likely to occur, which were verified by the higher yield of OA DESs during the preparation of CNCs.

Acknowledgments We appreciated Xiang Wang, Linlin Zheng and Haoyang Xu for building simulation models of the manuscript.

Authors' contribution Xuerong Bi performed the experiment and simulation. Jin Wen was a major contributor in analyzing data. Xuerong Bi wrote this manuscript. Chongwen Yu, Jin Wen, and Jiansheng Guo reviewed and revised the manuscript.

Funding This work is supported by China Agriculture Research System for Bast and Leaf Fiber Crops: CARS-16, and the Fundamental Research Funds for the Central Universities (2232021A-06).

Availability of data and materials All data generated during this study are included in this submitted article.

Declarations

Competing interests The authors declare no competing interests.

Ethics approval and consent to participate Not applicable.

Consent for publication Not applicable.

References

Abbott AP, Boothby D, Capper G, Davies DL, Rasheed RK (2004) Deep eutectic solvents formed between choline chloride and carboxylic acids: versatile alternatives to ionic liquids. J Am Chem Soc 126(29):9142–9147. https://doi.org/10.1021/ja048266j

Ahmadi R, Hemmateenejad B, Safavi A, Shojaeifard Z, Shahsavar A, Mohajeri A, Zolghadr AR (2018) Deep eutectic-water binary solvent associations investigated by vibrational spectroscopy and chemometrics. Phys Chem Chem Phys 20(27):18463–18473. https://doi.org/10.1039/C8CP00409A

Bader RFW (1992) Atoms in molecules. A quantum theory. Reihe: International series of monographs on chemistry, Vol. 22, Clarendon Press, Oxford

Bannwarth C, Ehlert S, Grimme S (2019) GFN2-xTB—an accurate and broadly parametrized self-consistent tight-binding quantum chemical method with multipole electrostatics and density-dependent dispersion contributions. J Chem Theory Comput 15(3):1652–1671. https://doi.org/10.1021/acs.jctc.8b01176

Becke AD (1988) Density-functional exchange-energy approximation with correct asymptotic-behavior. Phys Rev A 38(6):3098–3100. https://doi.org/10.1103/PhysRevA.38.3098

Cao B, Liu S, Du D, Xue Z, Fu H, Sun H (2016) Experiment and DFT studies on radioiodine removal and storage mechanism by imidazolium-based ionic liquid. J Mol Graph Model 64:51–59. https://doi.org/10.1016/j.jmgm.2015.10.008

Chen L, Zhu JY, Baez C, Kitin P, Elder T (2016) Highly thermal-stable and functional cellulose nanocrystals and nanofibrils produced using fully recyclable organic acids. Green Chem 18(13):3835–3843. https://doi.org/10.1039/C6GC00687F

Cheng M, Qin Z, Chen Y, Liu J, Ren Z (2017) Facile one-step extraction and oxidative carboxylation of cellulose nanocrystals through hydrothermal reaction by using mixed inorganic acids. Cellulose 24(8):3243–3254. https://doi.org/10.1007/s10570-017-1339-1

Dauber-Osguthorpe P, Roberts VA, Osguthorpe DJ, Wolff J, Genest M, Hagler AT (1988) Structure and energetics of ligand binding to proteins: *Escherichia coli* dihydrofolate reductase-trimethoprim, a drug-receptor system. Proteins 4(1):31–47. https://doi.org/10.1002/prot.340040106

Du H, Liu C, Mu X, Gong W, Lv D, Hong Y, Li B (2016) Preparation and characterization of thermally stable cellulose nanocrystals via a sustainable approach of $FeCl_3$-catalyzed formic acid hydrolysis. Cellulose 23(4):2389–2407. https://doi.org/10.1007/s10570-016-0963-5

Du H, Liu W, Zhang M, Si C, Zhang X, Li B (2019) Cellulose nanocrystals and cellulose nanofibrils based hydrogels for biomedical applications. Carbohydr Polym 209:130–144. https://doi.org/10.1016/j.carbpol.2019.01.020

Espinosa E, Molins E, Lecomte C (1998) Hydrogen bond strengths revealed by topological analyses of experimentally observed electron densities. Chem Phys Lett 285(3–4):170–173. https://doi.org/10.1016/S0009-2614(98)00036-0

French AD (2014) Idealized powder diffraction patterns for cellulose polymorphs. Cellulose 21(2):885–896. https://doi.org/10.1007/s10570-013-0030-4

French AD (2020) Increment in evolution of cellulose crystallinity analysis. Cellulose 27(10):5445–5448. https://doi.org/10.1007/s10570-020-03172-z

Frisch MJ, Pople JA, Binkley JS (1984) Self-consistent molecular-orbital methods 25 supplementary functions for Gaussian-basis sets. J Chem Phys 80(7):3265–3269. https://doi.org/10.1063/1.447079

Frisch MJ, Trucks GW, Schlegel HB, Scuseria GE, Robb MA, Cheeseman JR (2016) Gaussian 16, Revision A.01, Gaussian, Inc, Wallingford CT

Fu H, Wang X, Sang H, Hou Y, Chen X, Feng X (2020) Dissolution behavior of microcrystalline cellulose in DBU-based deep eutectic solvents: insights from spectroscopic investigation and quantum chemical calculations. J Mol Liq. https://doi.org/10.1016/j.molliq.2019.112140

Grimme S, Antony J, Ehrlich S, Krieg H (2010) A consistent and accurate ab initio parametrization of density functional dispersion correction (DFT-D) for the 94

elements H-Pu. J Chem Phys. https://doi.org/10.1063/1.3382344
Hariharan PC, Pople JA (1973) The influence of polarization functions on molecular orbital hydrogenation energies. Theor Chim Acta 28:213–222. https://doi.org/10.1007/BF00533485
Hehre WJ, Ditchfield R, Pople JA (1972) Self-consistent molecular orbital methods. XII. Further extensions of Gaussian-type basis sets for use in molecular orbital studies of organic molecules. J Chem Phys 56(5):2257–2261. https://doi.org/10.1063/1.1677527
Johnson ER, Keinan S, Mori-Sanchez P, Contreras-Garcia J, Cohen AJ, Yang W (2010) Revealing noncovalent interactions. J Am Chem Soc 132(18):6498–6506. https://doi.org/10.1021/ja100936w
Kalhor P, Zheng YZ, Ashraf H, Cao B, Yu ZW (2020) Influence of hydration on the structure and interactions of ethaline deep eutectic solvent: a spectroscopic and computational study. ChemPhysChem 21(10):995–1005. https://doi.org/10.1002/cphc.202000165
Kohn W, Becke AD, Parr RG (1996) Density functional theory of electronic structure. J Phys Chem 100(31):12974–12980. https://doi.org/10.1021/jp9606691
Lee CT, Yang WT, Parr RG (1988) Development of the Colle-Salvetti correlation-energy formula into a functional of the electron density. Phys Rev B 37(2):785–789. https://doi.org/10.1103/PhysRevB.37.785
Lim WL, Gunny AAN, Kasim FH, Gopinath SCB, Kamaludin NHI, Arbain D (2021) Cellulose nanocrystals from bleached rice straw pulp: acidic deep eutectic solvent versus sulphuric acid hydrolyses. Cellulose 28(10):6183–6199. https://doi.org/10.1007/s10570-021-03914-7
Liu Y, Wang H, Yu G, Yu Q, Li B, Mu X (2014) A novel approach for the preparation of nanocrystalline cellulose by using phosphotungstic acid. Carbohydr Polym 110:415–422. https://doi.org/10.1016/j.carbpol.2014.04.040
Liu Y, Chen W, Xia Q, Guo B, Wang Q, Liu S, Yu H (2017a) Efficient cleavage of lignin-carbohydrate complexes and ultrafast extraction of lignin oligomers from wood biomass by microwave-assisted treatment with deep eutectic solvent. Chemsuschem 10(8):1692–1700. https://doi.org/10.1002/cssc.201601795
Liu Y, Guo B, Xia Q, Meng J, Chen W, Liu S, Yu H (2017b) Efficient cleavage of strong hydrogen bonds in cotton by deep eutectic solvents and facile fabrication of cellulose nanocrystals in high yields. ACS Sustain Chem Eng 5(9):7623–7631. https://doi.org/10.1021/acssuschemeng.7b00954
Liu S, Zhang Q, Gou S, Zhang L, Wang Z (2021) Esterification of cellulose using carboxylic acid-based deep eutectic solvents to produce high-yield cellulose nanofibers. Carbohydr Polym. https://doi.org/10.1016/j.carbpol.2020.117018
Lu T, Chen F (2012) Multiwfn: a multifunctional wavefunction analyzer. J Comput Chem 33(5):580–592. https://doi.org/10.1002/jcc.22885
Lu T, Chen Q (2021) Interaction region indicator: a simple real space function clearly revealing both chemical bonds and weak interactions. Chem Methods 1(5):231–239. https://doi.org/10.1002/cmtd.202100007
Martínez L, Andrade R, Birgin EG, Martínez JM (2009) PACKMOL: a package for building initial configurations for molecular dynamics simulations. J Comput Chem 30(13):2157–2164. https://doi.org/10.1002/jcc.21224
Miao J, Yu Y, Jiang Z, Zhang L (2016) One-pot preparation of hydrophobic cellulose nanocrystals in an ionic liquid. Cellulose 23(2):1209–1219. https://doi.org/10.1007/s10570-016-0864-7
Mills G, Jónsson H (1994) Quantum and thermal effects in H_2 dissociative adsorption: evaluation of free energy barriers in multidimensional quantum systems. Phys Rev Lett 72(7):1124–1127. https://doi.org/10.1103/PhysRevLett.72.1124
Moon RJ, Martini A, Nairn J, Simonsen J, Youngblood J (2011) Cellulose nanomaterials review: structure, properties and nanocomposites. Chem Soc Rev 40(7):3941–3994. https://doi.org/10.1039/C0CS00108B
Neese F (2012) The ORCA program system. WIRES Comput Mol Sci 2(1):73–78. https://doi.org/10.1002/wcms.81
Neese F (2022) Software update: the ORCA program system—version 5.0. WIRES Comput Mol Sci. https://doi.org/10.1002/wcms.1606
Rajinipriya M, Nagalakshmaiah M, Robert M, Elkoun S (2018) Importance of agricultural and industrial waste in the field of nanocellulose and recent industrial developments of wood based nanocellulose: a review. ACS Sustain Chem Eng 6(3):2807–2828. https://doi.org/10.1021/acssuschemeng.7b03437
Selkälä T, Sirviö JA, Lorite GS, Liimatainen H (2016) Anionically stabilized cellulose nanofibrils through succinylation pretreatment in urea-lithium chloride deep eutectic solvent. Chemsuschem 9(21):3074–3083. https://doi.org/10.1002/cssc.201600903
Sirviö JA, Visanko M, Liimatainen H (2016) Acidic deep eutectic solvents as hydrolytic media for cellulose nanocrystal production. Biomacromol 17(9):3025–3032. https://doi.org/10.1021/acs.biomac.6b00910
Smirnov MA, Sokolova MP, Tolmachev DA, Vorobiov VK, Kasatkin IA, Smirnov NN, Yakimansky AV (2020) Green method for preparation of cellulose nanocrystals using deep eutectic solvent. Cellulose 27(8):4305–4317. https://doi.org/10.1007/s10570-020-03100-1
Spinella S, Maiorana A, Qian Q, Dawson NJ, Hepworth V, McCallum SA, Gross RA (2016) Concurrent cellulose hydrolysis and esterification to prepare a surface-modified cellulose nanocrystal decorated with carboxylic acid moieties. ACS Sustain Chem Eng 4(3):1538–1550. https://doi.org/10.1021/acssuschemeng.5b01489
Tognetti V, Cortona P, Adamo C (2008) A new parameter-free correlation functional based on an average atomic reduced density gradient analysis. J Chem Phys. https://doi.org/10.1063/1.2816137
Torlopov MA, Udoratina EV, Martakov IS, Sitnikov PA (2017) Cellulose nanocrystals prepared in $H_3PW_{12}O_{40}$-acetic acid system. Cellulose 24(5):2153–2162. https://doi.org/10.1007/s10570-017-1256-3
Xie H, Du H, Yang X, Si C (2018) Recent strategies in preparation of cellulose nanocrystals and cellulose nanofibrils derived from raw cellulose materials. Int J Polym Sci. https://doi.org/10.1155/2018/7923068

Xu W, Grenman H, Liu J, Kronlund D, Li B, Backman P, Xu C (2017) Mild oxalic-acid-catalyzed hydrolysis as a novel approach to prepare cellulose nanocrystals. Chemnanomat 3(2):109–119. https://doi.org/10.1002/cnma.201600347

Zhao Y, Truhlar DG (2008) Density functionals with broad applicability in chemistry. Acc Chem Res 41(2):157–167. https://doi.org/10.1021/ar700111a

Zheng YZ, Zhou Y, Liang Q, Chen DF, Guo R (2016) A theoretical study on the hydrogen-bonding interactions between flavonoids and ethanol/water. J Mol Model. https://doi.org/10.1007/s00894-016-2968-2